The NTUA Space Robot Emulator for Validation of Closed-Loop On-Orbit Servicing Tasks

A. Konstantinidis, I. Pelekoudas, O. Christidi-Loumpasefski, and E. G. Papadopoulos

National Technical University of Athens
School of Mechanical Engineering – Control Systems Laboratory
9 Heroon Polytechneiou Str., 15780, Athens, Greece
Email: {konstantinialex, peleioannis}@gmail.com, egpapado@central.ntua.gr

ABSTRACT

Space exploration and exploitation depend on the development of on-orbit robotic capabilities for tasks such as servicing of satellites, removing of orbital debris, or construction and maintenance of orbital assets. These complex tasks being performed in On-Orbit Servicing and Active Space Debris Removal missions, as well as the design and development of space systems including robotic manipulators, demand extensive on-earth planning, testing, and validation. To address such issues, the Control Systems Laboratory of NTUA has developed the air-bearing type Space Robot Emulator (SRE). In this paper, major upgrades to both the hardware and software of the NTUA SRE are described in detail. Two different closed-loop experiments in free-flying and free-floating modes showcase the new SRE functionality.

1 INTRODUCTION

Successes in space exploration have emphasized the growing importance of On-Orbit Servicing (OOS) in space programs around the world. Recently, active space debris removal missions (ASDR) have attracted the interest of most major space agencies. Future space missions for reusing and recycling the debris materials and/or satellite subsystems are being conceived.

To execute on-orbit tasks being impossible or too dangerous for humans, robotic manipulation is a preferable method. The capabilities of space robotic systems enable debris capture and several other OOS tasks, such as ORU replacement, repairs of damages, fuel replenishment and more.

The complex tasks being performed in OOS and ASDR missions, as well as the design and development of space systems including robotic manipulators, demand extensive on-earth planning, testing, and validation. As simulation is never enough, methods which allow even partial emulation of the space environment are of great importance. These methods include hardware-in-the-loop systems, parabolic flights, and neutral buoyancy facilities. If the planar motion of the robots is adequate, air bearings facilities present a high-fidelity emulation system, with a budget which can be adapted according to various requirements.

The Control Systems Laboratory (CSL) team at NTUA has developed a planar air bearing emulator since 2007; previous designs have been presented in [1-2]. The NTUA Space Robot Emulator (SRE) consists of a blue-black table on top of which robots can hover with negligent friction enabling microgravity emulation. To achieve more complex operations such as robot cooperation, docking, capture of a target and manipulation, the SRE consists of two active robots, see "Fig. 1" for one of them, and a passive one for the emulation of defunct satellites or space debris.

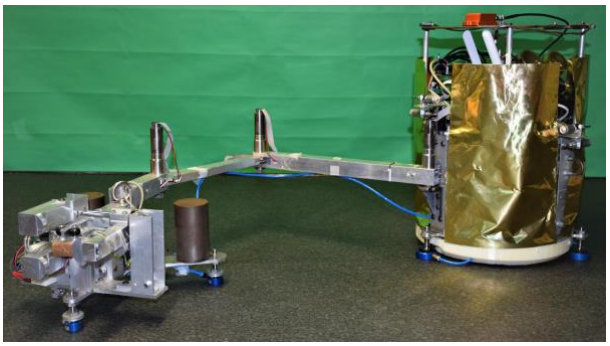

Figure 1. NTUA's Robotic Space Emulator "Cepheus."

In this paper, the development of the new NTUA SRE is presented. The major upgrades in its hardware and software, and its new functionalities, are described in detail. The system can be used in tasks that require closed-loop position or interaction control. To showcase the validation of closed-loop OOS tasks employing the upgraded SRE, two different experiments are performed and presented. In the first experiment, the task is the approach of a chaser robot towards a target system i.e., a space debris or a defunct satellite. Hence, the emulated space robot is in free-flying mode [3], during which the robot's base is controlled in closed-loop to follow specific Cartesian trajectories. In the second experiment, the emulated space robot is in free-floating mode [3], during which the new manipulator developed by NTUA, see "Fig. 3", is controlled in closed loop to successfully capture an emulated space debris. Both experiments showcase the functionality of the new NTUA Space Robot Emulator.

2 MECHANICAL DESIGN

The NTUA Space Robot Emulator, see "Fig. 1", consists of a granite table, two autonomous robots. The first, "Cassiopeia," is of older design, while the second, "Cepheus," is of newer design. The SRE includes an optical feedback system. The granite table has dimensions 2.2m x 1.8m x 0.3m, weighs approximately 3.5 tn, and has very low surface roughness (smaller than 5 μm) and very small inclination (smaller than 0.01º), thus allowing the simulation of frictionless microgravity conditions in two dimensions.

The suspension of the base above the granite table is achieved by three round air bearings, either of 25 or 40 mm in diameter, placed under the circular base and spaced at 120 degrees apart. Pressurized CO_2 is supplied through the porous material of the air bearings, thus creating a thin gas film (approximately 10 μm) between the base of the robot and the granite table, allowing frictionless planar motion. The CO_2 is provided to each of the three air bearings from a central CO_2 tank placed near the centre of mass of the base, weighing 1500 gr (when full) under pressure 60 bar (at 20ºC). The same tank provides the CO_2 necessary for the operation of thrusters.

The system was designed with modularity in mind, to be possible to integrate various components and subsystems with ease in changing them.

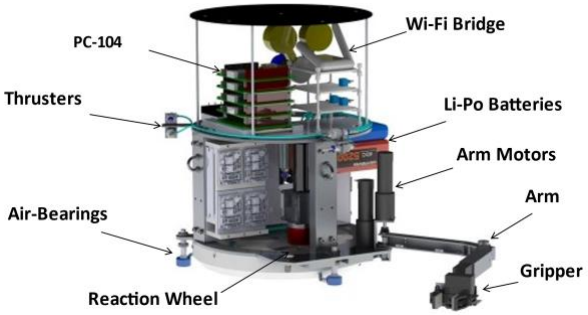

Figure 2. Parts of robot "Cepheus".

2.1 Subsystems

The autonomous robot "Cepheus" can be equipped with two different versions of robotic manipulator(s). In the first version, "Cepheus" has one or two manipulators of two-DoF, with their motors installed close to the main chassis, see "Fig. 2", as presented in [4]. In the second and upgraded version, the robot has a three-DoF manipulator with its motors installed on the joints to simplify the system, "Fig. 3". All manipulators are actuated by DC motors and commanded by the PC104. They have gearboxes for high torque output up to 6 Nm. In the first version, timing belts and pulleys are used to transfer the power of the motor to the appropriate joint.

At the end effector(s) of the manipulator(s) alternative types of grippers can be mounted. In the first version of robotic manipulator(s), predefined grippers were used that can apply a force up to 25 N, "Fig. 2".

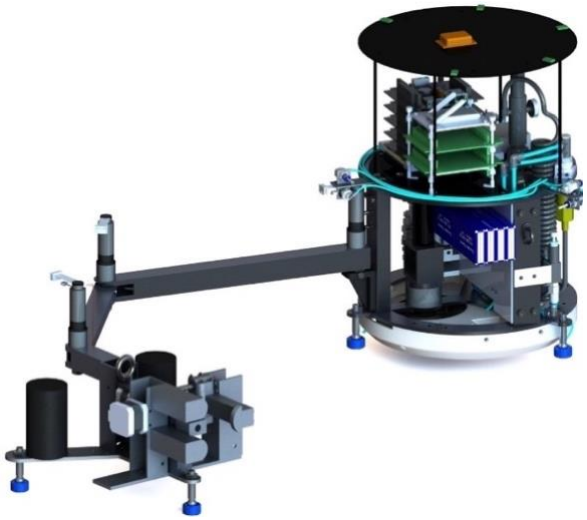

Figure 3. Upgraded robot "Cepheus" by NTUA.

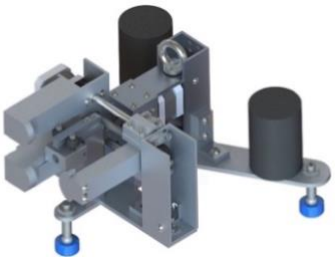

Figure 4. New heavy-duty gripper by NTUA.

For the second and upgraded version of the robot, a heavy-duty gripper is developed, shown in "Fig. 3" and "Fig. 4." The gripper weighs 6 kg and is capable of a rigid grasp with a target Launch Adapter Ring (LAR) up to 24 kg and moving it following the grasp. The gripper allows for the soft grasping during which it encloses the LAR between the claws of the gripper and hindering the decoupling of the target, applying force up to 50 N, and for hard grasping that ensures the locking and the stiff coupling of the two separate bodies, applying force up to 70 N. The gripper is actuated by linear nut and screw mechanisms with appropriate lead so that the gripper is non-back-drivable system, conserving system energy. In addition, this gripper is supported by air-bearings to facilitate the manipulator's work and make the experiments more realistic. The three-DoF manipulator is supported by a stiff base on the robot to be used even without the gripper at the end effector.

To realistically emulate the dynamic behaviour of the robots, it is important to increase the masses of the bodies involved in the experiments; therefore, a suitable extension base was attached to the active robot, which can be loaded with additional weights. Due to its weight, the system is lifted with a crane. New air-bearings have been added to the base, of 40 mm diameter, and the ability to lift and hover up to 60 kg load.

A base for a sloshing system has been designed and integrated on the robot to emulate the disturbances that are created due to accelerations. Similarly, another component of the satellites that can affect the dynamics

of the whole system, is the solar panel and for that reason an aluminium sheet with dimensions 250mm x 650mm x 1mm has been placed on one side of the robot sides, on a suitable detachable base with the two first bending natural frequencies equal to 1.96 Hz and 12.3 Hz.

2.2 Actuators

A thruster system is used to achieve base translational and rotational motion. The system consists of a single or double CO_2 tanks, a regulator that reduces the tank output pressure to 7 bar, and three pairs of on-off thrusters. An accurate system with strain gauges will provide feedback in real time about the actual force of the thrusters, closing the control loop. The three pairs of thrusters are placed peripherally mid-height around the base at 120 degrees from each other. Each pair consists of two opposed thrusters controlled by 6 electric 2-way on-off solenoid valves using Pulse Width Modulation (PWM).

A Reaction Wheel (RW) is used to control the orientation of the robot's base while reducing the CO_2 consumption by the thrusters. The wheel is actuated by a DC motor of maximum continuous torque on the output shaft at 0.088 Nm. The DC motor has an incremental encoder that provides the joint angle and the RW angular speed. The use of the RW makes the robot of the emulator resemble better an actual space robotic system, where the propulsion medium is limited in contrast to the practically infinite amount of electric energy available through the solar panels of the spacecraft. This is also true in the lab environment, as replenishing CO_2 takes time.

2.3 Sensors

The SRE employs a PhaseSpace motion capture system and can track up to three robots. Eight cameras placed around the table are tracking the LEDs on the top of each robot's base and provide absolute positions and orientations at 500 Hz and with high accuracy.

Force Sensitive Resistors (FSRs) are embedded on the claws of the grippers to measure gripper-applied forces. At the new gripper, new type of FSRs have been employed that have a range of measurement from 4.4 N up to 111 N and response time less than 5 μsec.

A Force-Torque Sensor has been used at the upgraded system to measure the torques and the forces in three axes. The sensor can be either fixed at the end effector between the gripper and the manipulator, or it can be integrated between the passive robot's frame and the LAR to estimate the loads that appear during impact docking. In missions where the two satellites must be coupled as in [5], the sensor can measure the forces of the contact between the probe and the drogue. The most useful feature of this sensor is its ability to allow for compliant control algorithms. It can measure forces up to 1200 N and torques up to 15 Nm with a sampling rate at 800 Hz and an error ±1 N and ±0.01 Nm.

An Inertial Measurement Unit (IMU) is also added in the upgraded system, and placed on top of the robot's base, providing its linear acceleration and angular velocity with high accuracy. IMU measurements are preferable in terms of linear acceleration since the double differentiation of the position by PhaseSpace is avoided. Moreover, it can detect the minute disturbances of the sloshing system during the movement. Its output frequency is up to 2 kHz measuring accelerations up to 20 g and noise ±4 μg.

Accelerometers are also part of the upgraded system, and their function is to give information about the acceleration and the velocity of the subsystems of the robots. A sampling rate up to 800 Hz is used, achieving high accuracy and low drift in measurements up to ±8g and 99 μg/√Hz noise. They are lightweight and easily integrated on the panel.

Hall Sensors are mounted on the moving parts that are actuated by motors with incremental encoders, i.e., at the joints of the manipulator and the linear screws of gripper, playing the role of a terminal switch

3 ELECTRIC AND ELECTRONIC DESIGN

The electrical and electronic design is based on previous work with some major additions [2]. The PC104 module, see "Fig. 5", has been upgraded to the i7 Intel core, with 2 cores at 1.7 GHz and 4 GB DDR3 SDRAM. Moreover, the motor drivers have been changed to a more accurate one, the ESCON 36/2 DC.

Figure 5. The upgraded PC104 module and the front I/O Cards that send commands to thrusters.

The gripper has its own electronics, a motor shield, and an Arduino, controlling the two stepper motors and reading the data of the FSRs and the Hall sensors. The accelerometers that are placed on the panel are also connected to an Arduino, which transfers the provided data to the PC104. Also, the electronic circuit controls the gas flow of the thrusters using Pulse Width Modulation (PWM) and actuates the 2-way on-off solenoid valves. This 0-5 V signal in PWM format from the PC104 results to a high power PWM voltage at 0-24 V. A components and signals schematic is presented in "Fig. 6".

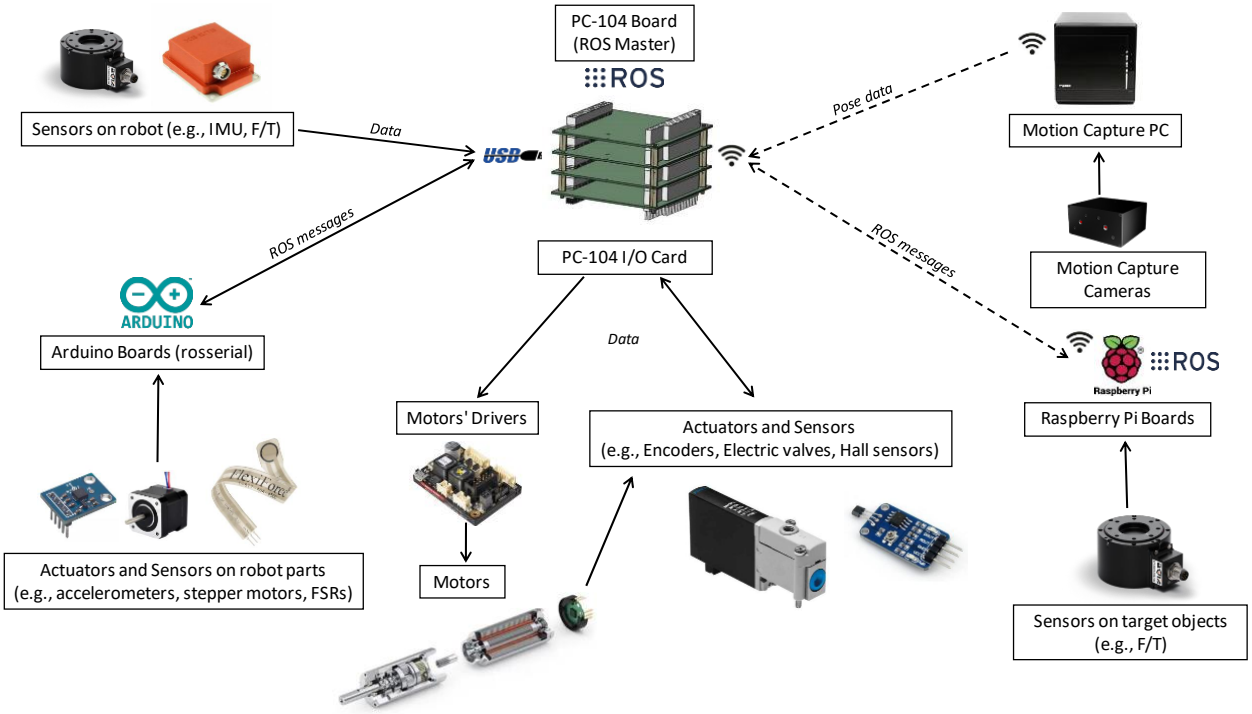

Figure 6. Components and signals schematic.

4 CONTROL SYSTEM

The closed-loop control system has been developed as an integral part of the of NTUA Space Robot Emulator and it employs several actuators and sensors.

The robotic arm and the RW joints are actuated via their DC motors, and they can be controlled in closed-loop. Currently, a PID controller is used to control the joint trajectories, either using the ROS Control, or the developed ROS node. Sensory feedback is provided by the encoders.

The end-effector(s) of the robotic arm(s) can be controlled in closed-loop to follow a desired trajectory in the Cartesian space. Currently, a PID controller is employed as part of the developed ROS nodes. The control loop can close either in joint-space employing inverse kinematics, or directly in Cartesian space. Sensory feedback is provided by the motion capture system, the IMU, and the encoders.

The robots' base is actuated using thrusters and the RW, and can be controlled in closed-loop. Currently, there are two controllers available as part of the developed ROS nodes to control the position and orientation of the robot's base; a simple PID and a Model-Based PD controller. Sensory feedback for the closed-loop control is provided by the motion capture system and the IMU.

Furthermore, the robot's base and the robotic arm(s) can be controlled simultaneously. Currently, there are three controllers available as part of the developed ROS nodes that allow simultaneous control of the position and orientation of the robot's base and the robotics arm(s) joints or end-effector's trajectories. These include a simple PID, a Coordinated Model-Based PD, and a Coordinated Impedance controller.

5 SOFTWARE

The SRE is a complex system that consists of a variety of computers i.e., PC104, PC, Raspberry Pi, and Arduino, that all deliver feedback data from the sensors that are responsible for, or they execute action commands.

Its complexity combined with its duty to perform various experiments with different configurations -that may include motion capture, force torque sensors, IMU sensors, accelerometers, PWM controllers for robot's thrusters, PID controllers for the arm joints and the reaction wheel- creates the necessity for software to be developed in a modular way and with room for customization to enable a wide range of experiments.

To best organize the software, the system utilizes ROS as the backbone of its structure and communications. ROS is an open-source software framework widely used in the robotics industry, with a significant and active community. It facilitates fast development using a structured communications layer that bridges the different hardware interfaces and minimizes the system complexity. A well-designed ROS system offers good separation of the low-level end that controls the hardware from the high-level end that performs the decision making (control).

5.1 Software Design

To demonstrate its autonomous capabilities, all closed-loop control calculations are being performed by the onboard PC104, running Ubuntu Linux distribution. This computer unit constitutes the master thread of the software controlling the system and the experiment sequences.

In pursuance of software separation and clear abstraction levels, the robotic system's operation has been separated from the experiment execution. The node responsible for the robot operation receives the configuration that provides the details about the set of sensors and actuators that must be initiated and the initial parameters for the pose, position, and orientation that the robot must reach before the experiment begins. Formerly, it launches all hardware interfaces of the chosen configuration and prepares the communication schema between all the threads of the distributed system with the main thread of operations. After the initialization is complete, the node starts to control the robot in the given position and pose until it receives a signal to release. Hereafter, the experiment thread takes over the control of the hardware.

For a specific experiment to be performed, the operator can use a dedicated ROS node containing the required control scheme. This node is independent from the rest of the software system in order to facilitate agile swaps between controllers or control schemes. The NTUA team has developed and has at its disposal various control ROS nodes for different scenarios, such as approaching of a target, docking, capture, berthing and manipulation. Any experiment thread can be terminated and restarted with different parameters, without the whole system and all its hardware interface threads having to be rebooted and reinitialized.

The modularity and abstraction that has been achieved, alleviates the efforts that a researcher must invest between experiments. Also, it has enabled the validation of the controller by mocking data from sensors and encoders to observe the controller's behaviour.

Furthermore, it is possible to replace the low-level end of the software with a simulation using Gazebo and its ROS integration, keeping the various control nodes as is. Finally, the design approach of having a main system operations node, makes it possible to configure and operate the experiment layout over a user interface, which is in the works.

6 VALIDATION OF OOS TASKS

To showcase the validation of closed-loop OOS tasks employing the upgraded SRE, two different experiments are performed and presented. In the first experiment, the task is the approach of a chaser robot towards a target system i.e., a space debris or a defunct satellite. Hence, the emulated space robot will be in free-flying mode [3], during which the robot's base is controlled in closed-loop to follow specific Cartesian trajectories. In the second experiment, the emulated space robot will be in free-floating mode [3], during which the new manipulator developed by NTUA will be controlled in closed loop to successfully capture an emulated space debris.

6.1 Task 1: Approach to a Target

6.1.1 Experimental Setup

The experimental setup during Task 1 of approaching the target system consists of the autonomous robot "Cepheus" in its upgraded version, i.e., with the new three-DoF manipulator. During this task, the manipulator joints are locked. The inertial parameters of "Cepheus" are given in "Table 1". The simulation model of the experimental setup is designed in SimScape, see "Fig. 7". Thrusters and RW are employed to control the position and orientation of the robot's base. The sensors used to perform the task are the PhaseSpace system and the IMU.

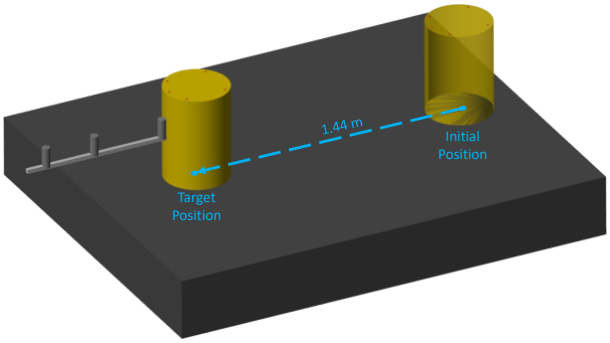

Figure 7. Model in Simscape and Trajectory for Task 1.

Table 1. Parameters of upgraded robot "Cepheus".

Link i	l_i (m)	r_i (m)	m_i (kg)	I_{zz} (kg m^2)
0	-	0.16	54	2.1831
1	0.26931	0.10069	0.2314	6.81e^{-3}
2	0.143	0.143	0.08797	6.4e^{-4}
3	0.17732	0.09768	6	9.972e^{-2}

6.1.2 Trajectory and Closed-Loop Control

To approach the target system at the target point, a pure translation trajectory $x_E(t)$ for the robot's base along the x-axis of the general coordinate system has been chosen. As shown in "Fig. 7", the robot is located at the one edge of the table and the target point is on the same y-position along the x-axis. The desired trajectory along the x-axis can be described by the following sequence: (i) a hold point at an initial position of 0.13 m, at 1.44 m from the target point, (ii) an approach with a constant acceleration 0.034 m/s^2 to reach a velocity of 5 cm/s, (iii) an approach with constant velocity 5 cm/s to reach the target point at 1.57 m. The desired trajectory along the y-axis and the desired orientation of the robot's base are equal to $y_E(t) = 0.72$ m and $q_E(t) = 0^o$, respectively. The base's desired pose $[x_E,\ y_E,\ q_E]^T$ is controlled with a PD controller. The duration of Task 1 is 30s.

6.1.3 *Experimental Results*

During approaching the target system in Task 1, the base follows accurately the desired Cartesian trajectories as shown in "Fig. 8". Specifically, the maximum relative error is less than 0.65%, see "Fig. 8.b". The relative error is calculated as the ratio of the absolute error in the x-position over the absolute relative initial distance 1.44 m. The maximum absolute errors in x- and y- position, see "Fig. 8.c", are less than 8 mm and 2 mm, respectively.

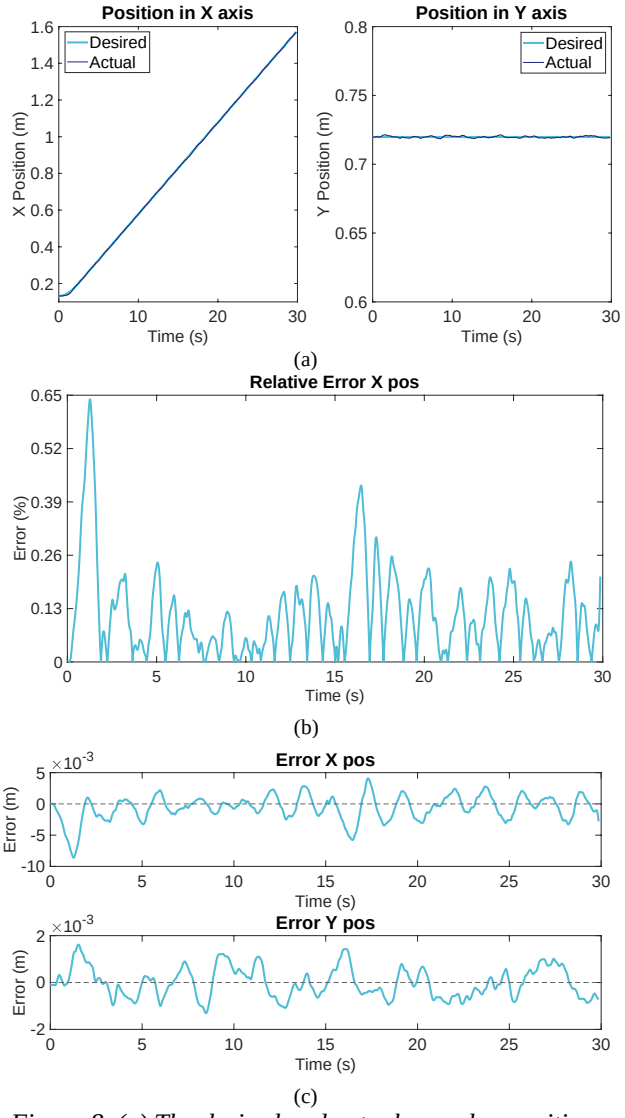

Figure 8. (a) The desired and actual x- and y- position, (b) the relative error in x-position, and (c) the absolute error in x- and y- position, for Task 1.

6.2 Task 2: Capture and Berthing

6.2.1 *Experimental Setup*

The experimental setup during Task 2 of capturing and berthing, see "Fig. 9" and "Fig. 12", consists of the autonomous robot "Cepheus" in the upgraded version i.e., with the new three-DoF manipulator and the new heavy-duty gripper, and the passive robot that emulates the 25 kg target system to be captured. The inertial parameters of "Cepheus" are given in "Table 1". The simulation model of the experimental setup is created in MSC ADAMS, see "Fig. 9".

The actuators employed are the motors of manipulator's joints and gripper. The sensors used are the manipulator's encoders and the gripper's FSR.

6.2.2 *Trajectory*

The Task 2 of capture and berthing task is divided in the following phases, shown also as snapshots in "Fig. 9" and "Fig. 12":

- Phase A: Final Approach towards Capturing (20 s)
  The gripper is positioned 100 mm away from the target and using only the manipulator is approaching the back surface of the LAR enclosing the latter between the claws, see "Fig. 11.a". During Phase A, the desired motion of the gripper is given in Cartesian space, and it is described by a fifth-degree polynomial $x_E(t)$ along the x-axis of the general coordinate system i.e., $\dot{y}_E(t), \dot{\theta}_E(t) = 0$. The desired angles are eventuated from $\dot{x}_E(t)$ using the system inverse dynamics.
- Phase B and C: Soft and Hard Grasping (30 s)
  The soft and the hard grasping of the target system are performed, see "Fig. 11.b" and "Fig. 11.c". The gripper is closing until a force of 40 N and 60 N for soft and hard capture, respectively, is read by the FSRs. Note that during the presented experiment, the gripper reaches the LAR aligned as shown in "Fig. 12". Nevertheless, in the case of misalignment, the gripper is capable of self-alignment to facilitate the capture, see "Fig. 13".
- Phase D: Trajectory towards Berthing (20 s)
  The manipulator achieves to transfer the target system at a 70 mm radical distance from the main frame of the robotic servicer and executes fine movements, see "Fig. 11.d". During Phase D, the desired motion of the gripper is given in joint space, and it is shown in "Fig. 14.a".
- Phase E: Berthing (10 s)
  The probe penetrates the berthing fixture which secures the conjunction of the two separate bodies, see "Fig. 11.e". During Phase E, the desired motion of the gripper is given in joint space, and it is shown in "Fig. 14.a". When Phase E and the securing of the system are completed, the manipulator is free to execute any other OOS or ASDR task.

6.2.3 *Closed-Loop Control*

The closed-loop control during the entire experiment closes in joint space employing a PD position controller. In the case the desired trajectory is in Cartesian space, as in Phase A, the desired joint rates are calculated employing the system dynamics [6].

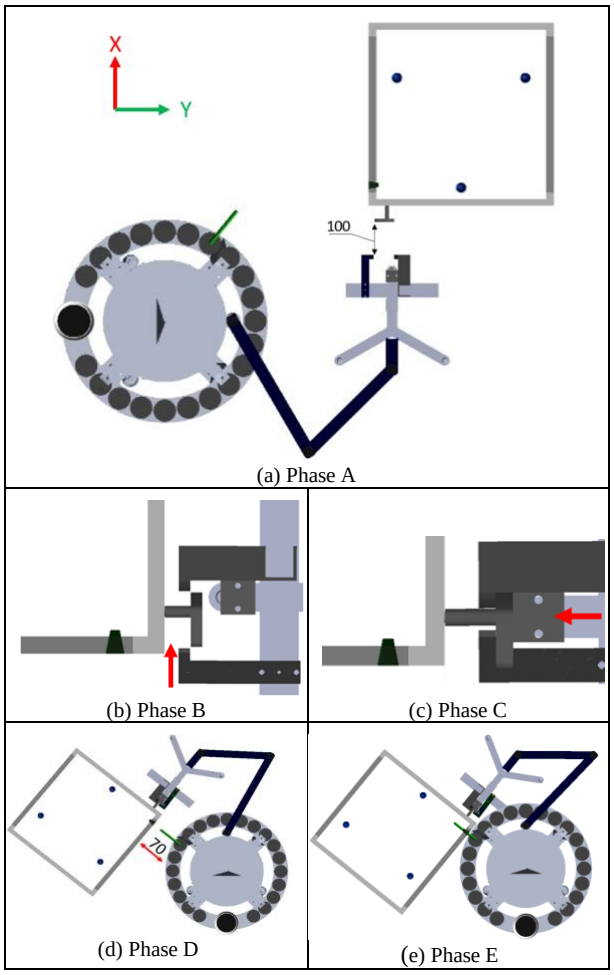

Figure 9. Model in ADAMS and snapshots for Task 2.

$$\dot{\mathbf{q}} = {}^{0}\mathbf{S}^{*-1}(\mathbf{q})\mathbf{E}^{-1}\begin{pmatrix}\dot{x}_E\\ \dot{y}_E\\ \dot{\theta}_E\end{pmatrix} \quad (1)$$

where $\mathbf{E}$ is a function of the rotation matrix of the base and ${}^{0}\mathbf{S}^{*}$ is the Generalized Jacobian, given by [6]

$${}^{0}\mathbf{S}^{*}(\mathbf{q}) = -\,{}^{0}\mathbf{J}^{*}_{11}\,{}^{0}D^{-1}\,{}^{0}\mathbf{D}_{q} + {}^{0}\mathbf{J}^{*}_{12} \quad (2)$$

where ${}^{0}D$, ${}^{0}\mathbf{D}_{q}$ are inertia-type matrices of the system, and ${}^{0}\mathbf{J}^{*}_{11}$ and ${}^{0}\mathbf{J}^{*}_{12}$ are based on system's Jacobian submatrices. All these matrices are functions of joint angles $\mathbf{q}$ and are given in [6].

The determinant of $\mathbf{S}(\mathbf{q})$ is used to identify a workspace free of dynamic singularities. When the determinant of $\mathbf{S}(\mathbf{q})$ is equal to zero the inverse problem has no solution; the system is singular.

6.2.4 Experimental Results

The snapshots of the system during the experiment of Task 2 are shown in "Fig. 12".

During Phase A of the final approach towards the capturing, the joints follow accurately the desired trajectories, see "Fig. 10.a". Subsequently, this leads to accurate movement in the Cartesian space with absolute errors less than 3 mm, see "Fig. 10.b", thus, the claws of the gripper successfully reach the desired position to capture the target.

During Phase B and C of the soft and hard capture of the target, respectively, the grasping forces, see "Fig. 11", are high enough to keep a stable coupling between the target and the manipulator.

During Phases D and E of berthing and securing the conjunction, the commanded trajectories of the joint angles are followed accurately, as shown in "Fig. 14", with a maximum absolute error 0.8°. Specifically, in "Fig. 14.a" and "Fig. 14.b", the desired and the actual joint angles, and the absolute errors of the joint angles, respectively, are presented.

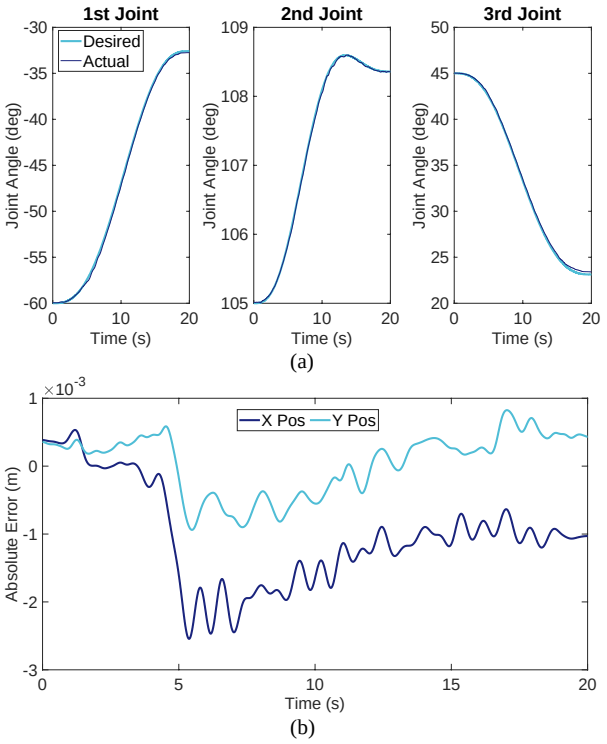

Figure 10. Phase A: (a) desired and actual joint angles and (b) absolute error of x- and y- position.

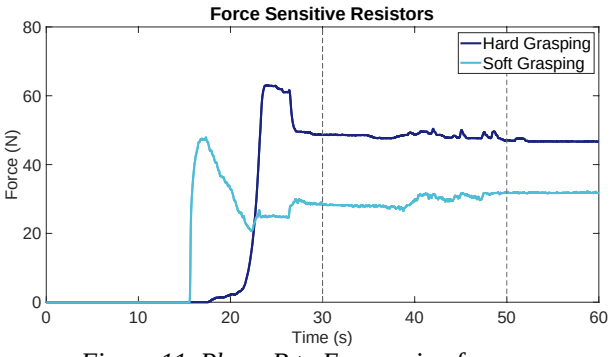

Figure 11. Phase B to E: grasping forces.

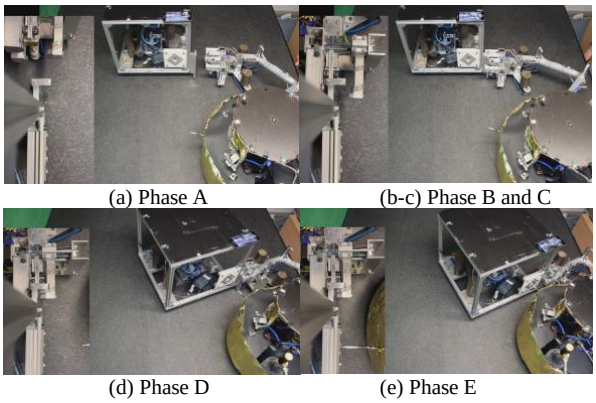

(a) Phase A (b-c) Phase B and C

(d) Phase D (e) Phase E

Figure 12. Snapshots during Experiment for Task 2 showing a series of phases during capture and berthing of a target.

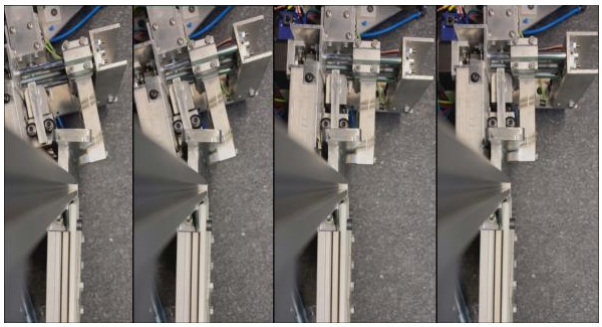

Figure 13. Capability of gripper self-alignment in case of target misalignment.

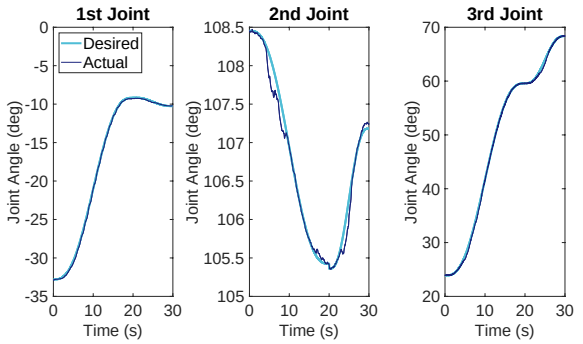

(a)

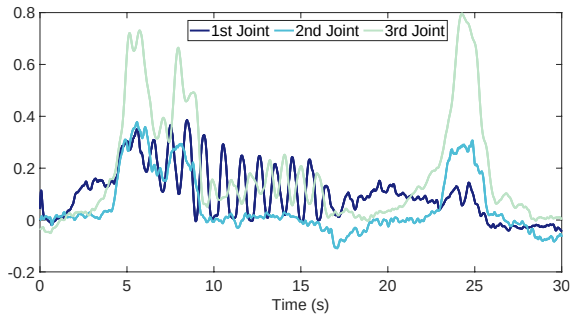

(b)

Figure 14. Phase D and E: (a) desired and actual joint angles and (b) absolute error of joint angles.

7 CONCLUSION

In this paper, the major hardware and software upgrades for the new NTUA Space Robot Emulator were presented, aiming at effective closed-loop control. The validation of closed-loop OOS tasks employing the new SRE was illustrated with two different experiments. In the first experiment, the chaser space robot actuated by the thrusters and RW in closed-loop control, successfully approached the target system and followed the desired Cartesian trajectory with high accuracy. In the second experiment, the emulated space robot was in free-floating mode, during which the new manipulator with the new gripper, both developed in house, was controlled in closed-loop to successfully capture an emulated space debris. Both experiments showcased the functionality of the new NTUA Space Robot Emulator and its effectiveness in the validation of OOS tasks.

8 AKNOWLEDGEMENTS

Olga Orsalia Christidi Loumpasefski was supported by an Onassis Foundation Scholarship.

9 REFERENCES

1. Papadopoulos, E. et al. (2011). The NTUA Space Robotic Emulator: Design and Experiments. *International Conference on Intelligent Robots and Systems (IROS) – Workshop on Space Robotics Simulation*, San Francisco, USA.

2. Machairas, K., Andreou, S., Paraskevas, I., and Papadopoulos, E. (2013). Extending the NTUA space robot emulator for validating complex on-orbit servicing tasks. *12th Symp. on Advanced Space Technologies in Robotics and Automation (ASTRA '13)*, ESA, ESTEC, Noordwijk, The Netherlands.

3. Papadopoulos, E., Aghili, F., Ma, O., and Lampariello, R. (2022). Robotic Manipulation and Capture in Space. *Frontiers: Robotics & AI - Space Robotics*.

4 Christidi-Loumpasefski, O.-O., Ntinos, C., and Papadopoulos, E. (2017). Analytical and Experimental Parameter Estimation for Free-Floating Space Manipulator Systems. *14th Symposium on Advanced Space Technologies in Robotics and Automation, (ASTRA '17)*, Scheltema, Leiden, the Netherlands.

5. Tomassini, A., et al., (2017). Towards a Standardized Grasping and Refuelling On-orbit Servicing for GEO Spacecraft. *Acta Astronautica*, Vol. 134, pp. 1–10.

6. Nanos, K., and Papadopoulos, E. (2015). Avoiding dynamic singularities in Cartesian motions of free-floating manipulators. *IEEE Transactions on Aerospace and Electronic Systems*, Vol. 51, No. 3, pp. 2305-2318.